RADAR PROPERTIES OF IMPACT EJECTA ON THE LUNAR MARIA: A MODEL FOR DEGRADATION AND AGE. C. Nypaver[1], B. J. Thomson[1], D. Burr[1], C. Fassett[2], C. Neish[3], W. Patterson[4], A. Stickle [4].[1]Department of Earth and Planetary Sciences, University of Tennessee, Knoxville, TN 37996. [2]NASA Marshall Spaceflight Center, Huntsville, AL 35808. [3]Department of Earth Sciences, The University of Western Ontario, London, Ontario, N6A 5B7. [4]Applied Physics Laboratory, Johns Hopkins University, Baltimore, MD 21218.

Introduction: Impact craters formed as the result of asteroid or comet impacts are ubiquitous features on the Moon and other planetary bodies. One natural by-product of an impact is ejecta excavated from the subsurface during the impact process. Fresh ejecta deposits on the lunar surface are an amalgamation of fine-grained regolith, angular rock fragments, and meter-scale boulders [1-2]; all of which scale with crater size [3]. In radar data, surface roughness registers as a circular "halo" around the crater [e.g., 4], and halo intensity varies among craters. Here, we focus on constraining the rate of ejecta degradation on the lunar maria by studying the radar signature of craters with a range of ages, and we hypothesize that ejecta halos fade at a quantifiable rate.

It has been shown that, with age, ejecta deposits degrade, angular fragments within the ejecta become rounded, and corresponding circular polarization ratios (CPRs) decrease [e.g., 5-6]. CPR is defined as the the ratio between power reflected in the same sense of circular polarization as that transmitted over the echo in the opposite sense [4], and is used in this case to quantify radar halo intensity. An age bin for impact craters of a similar diameter and degradation state can be estalished through a comparison of CPR and degradation state for craters within a particular size range. Indeed, previous work has resulted in the quantification of topographic degradation and the binning of craters into distinct age groups based on degradation state [7-8]. The degradation value for a given crater size bin can, therefore, be utilized to associate age and CPR for that bin. The primary mechanism for this quantified degradational process on the lunar surface is micrometeoroid bombardment [8-11]. In this study, we utilize ~15 m/pixel S-band (12.6 cm) radar data from the Miniature Radio Frequency (Mini-RF) instrument [12] aboard the Lunar Reconnaissance Orbiter (LRO) in conjunction with a previously established topographic degradation reference frame [8] to assess ejecta age and halo disappearance rate. Previous work in this area has involved interpreting CPR ratios for craters within the lunar maria in order to bin numerous individual craters into age groups based on degradation state [13]. We build upon their work by assessing craters in the same sample set, and by utilizing noise-mitigated Mini-RF data within our study of halo disappearance rate.

Data and Methodology: Individual craters chosen for analysis range from 0.8–3.0 km in diameter, and were covered by single Mini-RF S-band swaths. Mini-RF level 1 data swaths were imported from the PDS and manually processed via a suite of USGS ISIS3 scripts. These scripts apply SPICE kernels to the image swaths, and georectify the data. The level 1 data used in this study is of a higher spatial resolution than the level 2 data in the PDS. A radial CPR mean taken within this high-resolution data will produce a CPR profile that is less sensitive to a small number of anomalously high pixel values. Therefore, this use of this level 1 data, as opposed to level 2 data, in taking a radial mean, helps to mitigate speckle noise, and leads to clearer CPR profiles. While radial means provide sufficient data for the size range of craters presented here, radial medians more effectively show the mitigation of speckle noise in CPR profiles of larger craters and will be utilized moving forward. CPR profiles were extracted from each crater in our sample set and plotted against radial distance from the center of the crater (**Fig. 1C, F**). Previous modeling of the topographic evolution of simple craters on the lunar maria has demonstrated that the process of topographic degradation is most recognizeable with craters in the size range of 0.8–3.0 km, the size we use here [8].

Results: Our findings indicate CPR variability among craters of similar size and varying age. Moreover, the use of level 1 Mini-RF data for CPR extraction has helped mitigate speckle noise and has produced more precise median CPR plots than previous studies [13-14]. This aspect is a unique feature of our study, as the noise-reduced CPR data will allow for more constrained CPR readings for any given crater. CPR variations are also visible within individual craters (**Fig. 1C, F**). The highest CPR values in all sampled craters are associated with crater walls and rims. CPR values decrease with outward distance from the crater rim. Our initial findings are consistent with previous studies [7,13-14] which demonstrate that the ejecta of more degraded craters show lower CPR values, and the ejecta of fresh, less degraded craters show higher CPR values.

Discussion: At the lunar surface, blocky regolith can contribute to high radar brightness and increased CPR associated with the various features of an impact crater on the lunar maria [15]. Previous studies have shown that the highest CPR values are associated with crater rims and floors [11,13]. This increase in CPR is interpreted to be due to some combination of the pres-

ence of rocky debris, impact melt sheets, or a lack in fine-grained regolith on steep crater walls [4]. Although not as drastic as CPR values associated with interior parts of a crater, our radial CPR average plots (**Fig. 1C, F**) show that elevated CPR ratios are clearly visible in association with ejecta blankets. This increased CPR value is interpreted to be the result of sharp fragments of rock and impact breccia interspersed among the fine-grained regolith that makes up an ejecta blanket [15-16].

Based on our initial observations of the relationship between CPR and degradation state of impact craters on the lunar maria, we see evidence for a quantifiable rate of halo fading, and we anticipate that future work on this subject will help to fascilitate a better understanding and quantification of the rate at which ejecta halos fade.

Future work: In continuing work, we are assessing a sample set of approximately 7,000 craters using the methods laid out here. Given the results of this preliminary study, we find that such a study is warranted, and we anticipate that a larger sample set of craters, which spans the entire lunar maria, will give a more precise model of ejecta halo fading as a function of age.

References: [1] Koeberl C. (2013) In: Bobrowsky P.T. (eds) Encyclopedia of Natural Hazards. Encyclopedia of Earth Sciences Series. Springer, Dordrecht. [2] Melosh, H. J. (1996) *Oxfor*d *University Press*. [3] Bart, G. D., and H. J. Melosh (2007) *Geophys. Res. Lett.*, 34, L07203, [4] Campbell, B. A. (2012) *J. Geophys. Res.*, 117, E06008. [5] Bell, S. W. et al. (2012) *J. Geophys. Res*., 117, E00H30. [6] Desai, A.J. et al. (2014) *Current Science*, vol. 107, pp. 824-831. [7] Neish, C. D., et. al (2013) *J. Geophys. Res. Planets*, 118, 2247–2261 [8] Fassett, C. I., and B. J. Thomson (2014) *J. Geophys. Res. Planets*, 119, 2255–2271. [9] Ross, H. P. (1968) *J. Geophys. Res*., 73, 1343–1354. [10] Soderblom, L. A. (1970) *J. Geophys. Res.*, 75, 2655–2661. [11] Jawin, E. R et al. (2014) *J. Geophys. Res. Planets*, 119, 2331–2348. [12] Raney, R. K., et al. (2011), *Proc. IEEE*, 99(5), 808–823 [13] King, I.R. et al.(2017) *Lunar Planet. Sci. Conf. 48th*, abstract 1612. [14] A.M. Stickle et, al. (2016). *In Icarus*, Volume 273 , Pages 224-236, ISSN 0019-1035, [15] Fa, W., and Y. Cai (2013) *J. Geophys. Res. Planets*, 118, 1582–1608. [16] Thomson, B. J. et al. (2012a) *Lunar Planet. Sci. Conf. 43rd*, abstract 2014

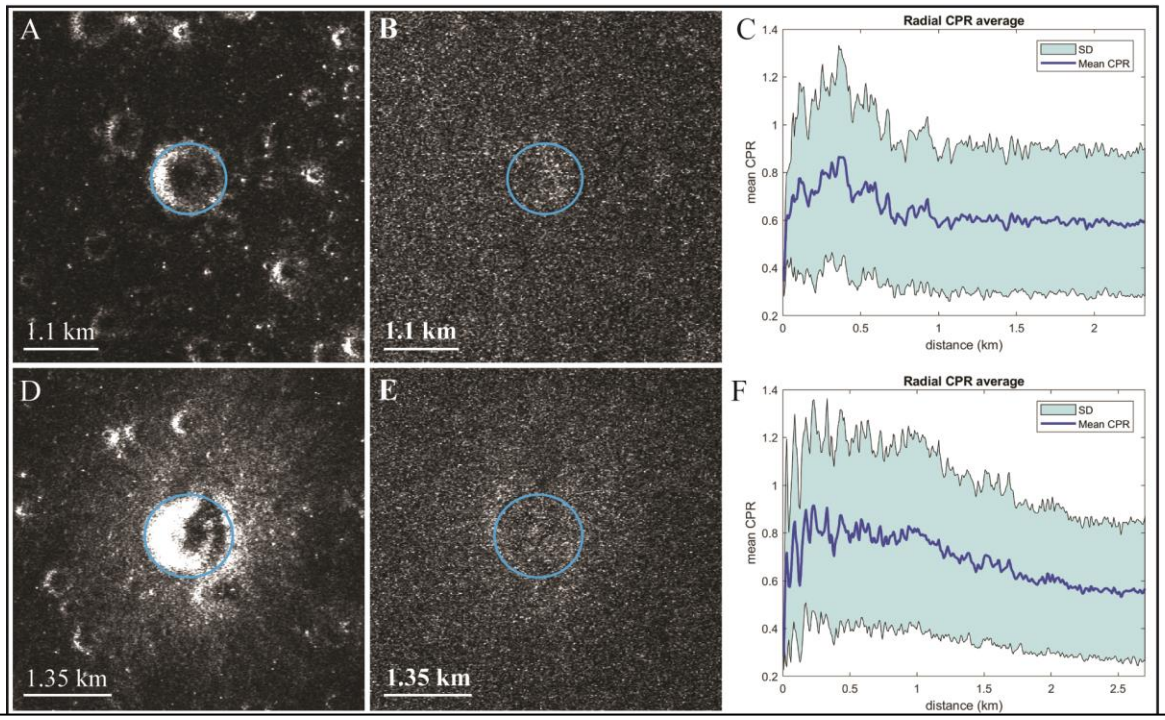

Figure 1 (**A-B**): Example of a simple 1.1-km crater possessing a visually muted radar halo in (**A**) Mini-Rf level-1 S1 data and in (**B**) processed Mini-RF level 1 CPR data. Visible within the radial CPR average plot for this crater (**C**) is a CPR maxima of ~0.9 associated with the crater rim (0.675 km), and a rapid decrease in CPR with increased distance from the crater rim. Figures **D-E** show a simple 1.35 km crater with a bright radar halo in (**D**) Mini-Rf level-1 S1 data and in (**E**) processed level 1 CPR data. The radial CPR average plot for this crater (**F**) shows a CPR peak of ~0.9 associated with the crater rim (0.581 km), and a much more gradual decline in CPR with distance from the crater rim. Blue rings depict approximate crater rims in all images. The dark blue line in each graph represents the mean CPR, while the teal-shaded area represents the standard deviation (labeled "SD" in the graph legend). CPR plots for both craters are extrapolated out to 4 crater radii.